

# Transmission magnitude and phase control for polarization-preserving reflectionless metasurfaces

Do-Hoon Kwon,<sup>1,\*</sup> Grigori Ptitsyn,<sup>2</sup> Ana Díaz-Rubio,<sup>2</sup> and Sergei A. Tretyakov<sup>2</sup>

<sup>1</sup>*Department of Electrical and Computer Engineering,*

*University of Massachusetts Amherst, Amherst, Massachusetts 01003, USA*

<sup>2</sup>*Department of Electronics and Nanoengineering, Aalto University, P.O. Box 15500, 00076 Aalto, Finland*

For transmissive applications of electromagnetic metasurfaces, an array of subwavelength Huygens' meta-atoms are typically used to eliminate reflection and achieve a high transmission power efficiency together with a wide transmission phase coverage. We show that the underlying principle of low reflection and full control over transmission is asymmetric scattering into the specular reflection and transmission directions that results from a superposition of symmetric and anti-symmetric scattering components, with Huygens' meta-atoms being one example configuration. Available for oblique illumination in TM polarization, a meta-atom configuration comprising normal and tangential electric polarizations is presented, which is capable of reflectionless, full-power transmission and a  $2\pi$  transmission phase coverage as well as full absorption. For lossy metasurfaces, we show that a complete phase coverage is still available for reflectionless designs for any value of absorptance. Numerical examples in the microwave and optical regimes are provided.

## I. INTRODUCTION

Presented as two-dimensional equivalents of volumetric metamaterials [1], metasurfaces have attracted a significant interest in recent years. Metasurfaces are typically realized as a doubly periodic array of small polarizable particles over a sub-wavelength thickness. With a distinct advantage of low loss over volumetric metamaterials, a wide range of novel reflection, transmission, and absorption applications ranging from microwave to optical frequencies have been reported [2–6].

There are a host of metasurface applications in the transmission mode. Based on the phased array antenna principle [7] and the generalized law of refraction [8], a linear gradient of transmission phase imparted on the transmitted wave can bend an incident beam or plane wave in an anomalous direction [9–12]. A flat focusing lens is obtained by spatially nonlinear transmission phase distributions [13–16]. Local modulation of transmission amplitude and/or phase leads to holograms [17–19]. As polarization transformers, thin metasurfaces can replace electrically thick wave plates by assigning distinct transmission phases to two orthogonal polarization components [20–22].

A high transmission magnitude toward unity and a wide transmission phase range toward  $2\pi$  are highly desirable for high-efficiency operation of transmitted wave shaping. At optical frequencies, a single layer of plasmonic or dielectric resonant particles are commonly adopted for transmissive metasurfaces, owing to relative ease of fabrication. It was recognized that an infinitesimally thin layer of electrically polarizable particles support a complete  $2\pi$  range for the cross-polarized transmission phase, but not for the co-polarized transmission. Accordingly, formalization of the generalized laws of reflection and refraction as well as their experimental demonstrations were performed for the cross-polarized components scattered by V-shaped optical antennas under linearly polarized illuminations [8, 23], albeit at a low cross-polarized transmission efficiency. It was later revealed that the maxi-

mum cross-coupled power efficiency is 25% [13]. Another approach to achieve a  $2\pi$  transmission phase coverage is to exploit the Pancharatnam-Berry phase together with circularly polarized illuminations. For the transmitted circularly polarized wave of the opposite handedness, the phase can be adjusted simply by rotating the principal axes of a wave-plate element [14, 18, 24]. Still, this approach involves cross-polarized transmitted waves and a completely reflectionless operation is not possible.

For polarization-preserving applications to date, reflectionless metasurfaces with a complete  $2\pi$  transmission phase coverage are based on Huygens' meta-atoms [9, 12, 25–27]. A Huygens' meta-atom is designed such that an orthogonal set of tangential electric and magnetic dipole moments are induced upon external plane-wave excitation. When the two induced dipoles satisfy a balanced condition, full transmission and zero reflection can be obtained for lossless cases with the transmission phase that can be designed to have any value within a complete  $2\pi$  range. In the microwave regime, short conductor traces are typically used for electric dipoles. For equivalent magnetic dipoles, either metallic ring resonators [9] or conductor traces in a multi-layer dielectric substrate [21, 28, 29] are utilized. **Utilizing a combination of continuous and discrete printed multi-layer conductor traces for realizing Huygens' meta-atoms, microwave transmissive metamaterials for lenses, beam deflectors, and vortex beam generators with efficiencies as high as 91% have been demonstrated [30–32].** In the optics regime, a dielectric resonator meta-atom can be designed to support both electric and equivalent magnetic polarization currents at the same wavelength [12, 25, 26]. It is challenging to design induced electric and magnetic polarizations to satisfy a balanced amplitude and phase relation at the same frequency due to strong mutual coupling between them. Furthermore, the bandwidth of the magnetic resonance tends to be narrower than that of the electric one. At microwave frequencies, the length and shape of a thin conductor wire may be designed to strike a balance between the induced electric and equivalent magnetic dipole moments. This approach has been demonstrated with a circularly polarized Huygens spiral particle in [33].

In this paper, a fundamental principle behind full power

\* dhkwon@umass.edu

transmission with a complete phase coverage is investigated for polarization-preserving metasurfaces. It is shown that generation of an anti-symmetric scattering component by the induced polarizations and its destructive interference with the symmetric scattering component in nullifying the total reflected wave is the key design principle. In Huygens' metasurfaces, a tangential magnetic dipole moment provides the necessary anti-symmetric scattering. However, it is not the only possible source of anti-symmetric scattering. It has been recently shown that the effect of a tangential magnetic polarization can be equivalently generated by a spatially varying normal electric polarization [34]. Taking advantage of this equivalence, a meta-atom configuration comprising entirely of electric dipole moments that is capable of full transmission with a  $2\pi$  phase coverage is presented. The new reflectionless metasurface configuration is available for oblique illuminations in the TM polarization. Here, the anti-symmetric scattering is provided by an electric dipole that is polarized normal to the metasurface.

When a combination of tangential and normal induced electric dipoles are realized with a tilted electric dipole meta-atom, the identical frequency dispersion of the two orthogonal dipole moments permits *dispersionless* full transmission at a *fixed* oblique incidence angle. Furthermore, the resonance of a dipole meta-atom can be tuned in order to achieve a full transmission phase coverage. It is known that metallic gratings having an array of narrow slits or apertures allow *dispersionless* broadband extraordinary transmission under a TM-polarized illumination at some fixed oblique angle [35–37]. The underlying physics of this broadband full transmission is an impedance match between an oblique TM-polarized illumination and a propagating mode inside a slit [36]. In contrast, the dispersionless transmission property of a tilted dipole array in this study is of geometrical nature of the dipole pattern null directions. This allows the frequency dispersion of a dipole meta-atom to be exploited for transmission phase synthesis.

Furthermore, the inevitable effect of absorption in practical metasurface realizations on the transmission phase coverage is discussed. It is revealed that a complete  $2\pi$  range of transmission coverage is still available regardless of the amount of loss for reflectionless designs. Finally, illustrative uniform metasurface design examples are provided and analyzed. As a microwave example, a tilted thin conducting strip dipole array is shown for providing full transmission and a complete phase coverage. As its lossy variant, an impedance-loaded strip dipole array is analyzed for full phase coverage as well as for perfect absorption. For an example in the optical regime, high transmission and full phase coverage by an all-dielectric metasurface composed of dielectric bars of rectangular cross section are demonstrated.

In the following time-harmonic analysis at an angular frequency  $\omega$ , an  $e^{j\omega t}$  time dependence is assumed and suppressed.

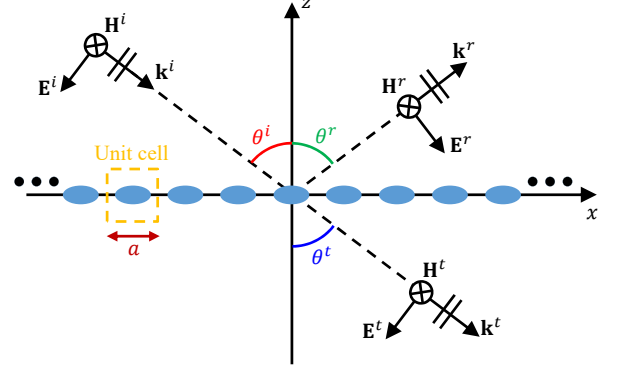


FIG. 1. Reflection and transmission of a TM-polarized plane wave by a metasurface in the  $xy$ -plane situated in free space.

## II. TM-MODE REFLECTION AND TRANSMISSION

We treat a uniform (non-gradient), single-layer metasurface in free space. As will be shown, lossless metasurfaces supporting electric polarizations only are capable of full-power transmission in the TM polarization. Figure 1 illustrates a planar metasurface in the  $xy$ -plane illuminated by a TM-polarized plane wave propagating in the  $xz$ -plane with an angle of incidence  $\theta^i$ . The unit-cell dimensions are  $a$  and  $b$  in the  $x$ - and  $y$ -axis directions, respectively. The dimensions are set such that only the fundamental Floquet mode fields propagates away from the metasurface. Away from the metasurface where all evanescent higher-order Floquet mode waves vanish, the incident, reflected, and transmitted electric fields can be written as

$$\mathbf{E}^p = \mathbf{E}_0^p e^{-j(k_x^p x + k_z^p z)}; \quad p = i, r, t, \quad (1)$$

where the superscripts ‘i,’ ‘r,’ and ‘t’ denote the incident, reflected, and transmitted fields, respectively, and  $\mathbf{E}_0^p$  denotes the corresponding E-field vector amplitude. The associated wave vectors in the  $xz$ -plane are given by  $(k_x^i, k_z^i) = (k \sin \theta^i, -k \cos \theta^i)$ ,  $(k_x^r, k_z^r) = (k \sin \theta^r, k \cos \theta^r)$ , and  $(k_x^t, k_z^t) = (k \sin \theta^t, -k \cos \theta^t)$ , with  $k$  denoting the free-space wavenumber. All magnetic fields are  $y$ -polarized. For a uniform metasurface, all three angles are the same ( $\theta^i = \theta^r = \theta^t$ ).

For metasurfaces that do not scatter cross-polarized fields, the transmission and reflection in Fig. 1 can be described using a two-port network in terms of  $S$ -parameters, with plane-wave ports 1 and 2 defined in positive- and negative- $z$  half spaces. With the phase reference planes for both ports set to  $z = 0$ , the reflection coefficient  $r = S_{11}$  and the transmission coefficient  $t = S_{21}$  are defined as the ratios of tangential E-field amplitudes as

$$r = \frac{\hat{x} \cdot \mathbf{E}_0^r}{\hat{x} \cdot \mathbf{E}_0^i} = \frac{E_{0x}^r}{E_{0x}^i}, \quad t = \frac{\hat{x} \cdot \mathbf{E}_0^t}{\hat{x} \cdot \mathbf{E}_0^i} = \frac{E_{0x}^t}{E_{0x}^i}. \quad (2)$$

There are three elemental dipole meta-atoms that scatter TM-polarized fields, which are assumed to be excited by the incident wave. They are two orthogonal electric dipoles in

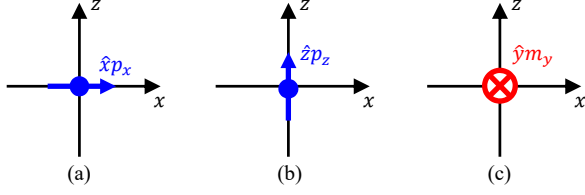


FIG. 2. Three elemental dipole meta-atoms for TM-polarization reflection and scattering. (a) An  $x$ -directed electric dipole. (b) A  $z$ -directed electric dipole. (c) A  $y$ -directed magnetic dipole.

the plane of incidence (the  $xz$ -plane) and one magnetic dipole that is directed normal to the plane of incidence, as shown in Fig. 2. Each point dipole is positioned at the coordinate origin. A general meta-atom can be represented as a superposition of these three dipoles. The scattering characteristics of the elemental dipoles are discussed next.

### A. Symmetric scattering

A planar array of the tangential electric dipole  $\hat{x}p_x$  in Fig. 2(a) radiates plane waves symmetrically into  $z \rightarrow \pm\infty$ . The scattered E-field amplitudes,  $\mathbf{E}_0^{s,r}$  and  $\mathbf{E}_0^{s,t}$ , in the reflection and transmission directions, respectively, are given by

$$\mathbf{E}_0^{s,r} = \frac{j\omega\eta}{2S \cos \theta^i} \hat{k}^r \times \hat{k}^r \times \hat{x}p_x, \quad (3)$$

$$\mathbf{E}_0^{s,t} = \frac{j\omega\eta}{2S \cos \theta^i} \hat{k}^t \times \hat{k}^t \times \hat{x}p_x, \quad (4)$$

where  $\eta \approx 377 \Omega$  is the free-space intrinsic impedance and  $S = ab$  represents the unit-cell area in the  $xy$ -plane. Also,  $\hat{k}^r = \mathbf{k}^r/k$  and  $\hat{k}^t = \mathbf{k}^t/k$  are the unit vectors in their respective propagation directions. The tangential components of  $\mathbf{E}_0^{s,r}$  and  $\mathbf{E}_0^{s,t}$  are the same (symmetric). Denoting this value by  $E_{0x}^{s,s}$ , we find

$$E_{0x}^{s,s} = \hat{x} \cdot \mathbf{E}_0^{s,r} = \hat{x} \cdot \mathbf{E}_0^{s,t} = -\frac{j\omega\eta p_x}{2S} \cos \theta^i. \quad (5)$$

These scattered field amplitudes could be cast in terms of the surface-averaged electric polarization current density  $J_x = j\omega p_x/S$ .

### B. Anti-symmetric scattering

Both a normal electric dipole [Fig. 2(b)] and a tangential magnetic dipole [Fig. 2(c)] radiate anti-symmetrically into  $z \rightarrow \pm\infty$ . First, the  $z$ -directed electric dipole meta-atom generates scattered plane waves in the  $\hat{k}^r$ ,  $\hat{k}^t$  directions with the E-field amplitudes given by

$$\mathbf{E}_0^{s,r} = \frac{j\omega\eta}{2S \cos \theta^i} \hat{k}^r \times \hat{k}^r \times \hat{z}p_z, \quad (6)$$

$$\mathbf{E}_0^{s,t} = \frac{j\omega\eta}{2S \cos \theta^i} \hat{k}^t \times \hat{k}^t \times \hat{z}p_z. \quad (7)$$

The  $x$ -components of these two vectors are different by sign (anti-symmetric). Denoting the anti-symmetric component by  $E_{0x}^{s,a}$ , we find

$$E_{0x}^{s,a} = \hat{x} \cdot \mathbf{E}_0^{s,r} = -\hat{x} \cdot \mathbf{E}_0^{s,t} = \frac{j\omega\eta p_z}{2S} \sin \theta^i. \quad (8)$$

Next, a planar array of the  $y$ -directed magnetic dipole meta-atom in Fig. 2(c) creates the E-field amplitudes for the scattered plane waves given by

$$\mathbf{E}_0^{s,r} = \frac{j\omega}{2S \cos \theta^i} \hat{k}^r \times \hat{y}m_y, \quad (9)$$

$$\mathbf{E}_0^{s,t} = \frac{j\omega}{2S \cos \theta^i} \hat{k}^t \times \hat{y}m_y. \quad (10)$$

The anti-symmetric  $x$ -components can be written as

$$E_{0x}^{s,a} = \hat{x} \cdot \mathbf{E}_0^{s,r} = -\hat{x} \cdot \mathbf{E}_0^{s,t} = -\frac{j\omega m_y}{2S}. \quad (11)$$

The field amplitudes can also be written in terms of the surface-averaged polarization current densities,  $J_z = j\omega p_z/S$  and  $M_y = j\omega m_y/S$ .

### C. Transmission and reflection coefficients for total fields

Infinitely thin metasurfaces can support tangential electric polarizations only and the resulting symmetric scattering is the reason for low transmission power efficiencies for polarization-preserving designs [13]. For Huygens' metasurfaces, the asymmetric scattering enabled by a combination of orthogonally directed tangential electric and magnetic dipoles allows full transmission [12, 26]. In order to support an equivalent magnetic dipole realized using a circulating electric polarization, a Huygens' metasurface cannot have a vanishingly small thickness.

We note that the anti-symmetric scattering may be provided by a normal electric dipole rather than a tangential magnetic dipole. Regardless of the origin of anti-symmetric radiation, the total tangential E-field components for the reflected and transmitted waves can be written as a superposition as

$$E_{0x}^r = E_{0x}^{s,s} + E_{0x}^{s,a}, \quad E_{0x}^t = E_{0x}^{i,s} + E_{0x}^{s,s} - E_{0x}^{s,a}, \quad (12)$$

where the symmetric component  $E_{0x}^{s,s}$  is given by (5). The anti-symmetric component  $E_{0x}^{s,a}$  is given by (8) if  $\hat{z}p_z$  is used and by (11) if  $\hat{y}m_y$  is used. Then, we can write the reflection and transmission coefficients as

$$r = \frac{E_{0x}^r}{E_{0x}^i} = r_s + r_a; \quad r_s = \frac{E_{0x}^{s,s}}{E_{0x}^i}, \quad r_a = \frac{E_{0x}^{s,a}}{E_{0x}^i}, \quad (13)$$

$$t = \frac{E_{0x}^t}{E_{0x}^i} = t_s - r_a, \quad t_s = 1 + r_s, \quad (14)$$

where  $r_s$  and  $r_a$  represent reflection coefficients for the symmetric and anti-symmetric components, respectively. In (14),  $t_s$  denotes the transmission coefficient in the absence of anti-symmetric scattering.

### III. TRANSMISSION PHASE FOR LOSSLESS, REFLECTIONLESS METASURFACES

For lossless metasurfaces, power conservation requires  $|r|^2 + |t|^2 = 1$ . In terms of  $t_s$  and  $r_a$ , this condition translates into

$$|t_s|^2 + |r_a|^2 - \text{Re}\{t_s + r_a\} = 0. \quad (15)$$

Now, we require a reflectionless operation for maximum power transmission ( $r = 0$ ), or set  $r_a = 1 - t_s$ . Using this condition in (15), we obtain  $|t_s|^2 = \text{Re}\{t_s\}$ , which can be rewritten as

$$|t_s| = \cos \phi_{t_s}, \quad (16)$$

if we write  $t_s = |t_s|e^{j\phi_{t_s}}$  (i.e.,  $\angle t_s = \phi_{t_s}$ ). Using (16), the total transmission coefficient is found to be

$$\begin{aligned} t &= t_s - r_a = 2t_s - 1 = 2\text{Re}\{t_s\} - 1 + j2\text{Im}\{t_s\} \\ &= 2|t_s| \cos \phi_{t_s} - 1 + j2|t_s| \sin \phi_{t_s} \\ &= \cos 2\phi_{t_s} + j \sin 2\phi_{t_s} = e^{j2\phi_{t_s}}. \end{aligned} \quad (17)$$

Hence, we find

$$\angle t = 2\phi_{t_s}. \quad (18)$$

Starting from  $t = 1 + 2r_s$  instead, a similar analysis finds

$$\angle t = 2\phi_{r_s} + \pi, \quad (19)$$

where  $\phi_{r_s} = \angle r_s$ . From (18)–(19), we find that the transmission phase range is twice those of the transmission and reflection coefficients of the symmetric component. The magnitude of the transmission coefficient is unity due to full transmission, as it should be for lossless, reflectionless metasurfaces.

Let us assume no bianisotropy and a standard Lorentz frequency dispersion for the lossless electric polarizability  $\alpha_{ee}$  for the horizontal electric dipole  $p_x$ . The polarizability can be modeled as [38, 39]

$$\alpha_{ee} = \frac{A_e}{\omega_e^2 - \omega^2}, \quad (20)$$

where  $A_e$  is the resonance strength coefficient related to the plasma frequency and  $\omega_e$  is the electric resonance frequency. The polarizability  $\alpha_{ee}$  relates the induced dipole moment to the local excitation field at the dipole location. By defining an effective polarizability  $\hat{\alpha}_{ee}$  for the dipole in an array environment, the induced dipole moment can be written relative to the incident field as  $p_x = \hat{\alpha}_{ee} E_{0x}^i$ . It is known that the two polarizabilities are related by [39]

$$\frac{1}{\eta \hat{\alpha}_{ee}} = \frac{1}{\eta \alpha_{ee}} + \frac{j\omega}{2S} \cos \theta^i \quad (21)$$

in the TM polarization. Using (5), (20), and (21), the expression for  $r_s$  is found to be

$$r_s = -j \frac{\omega \cos \theta^i}{2S} \left( \frac{\omega_e^2 - \omega^2}{\eta A_e} + \frac{j\omega}{2S} \cos \theta^i \right)^{-1}. \quad (22)$$

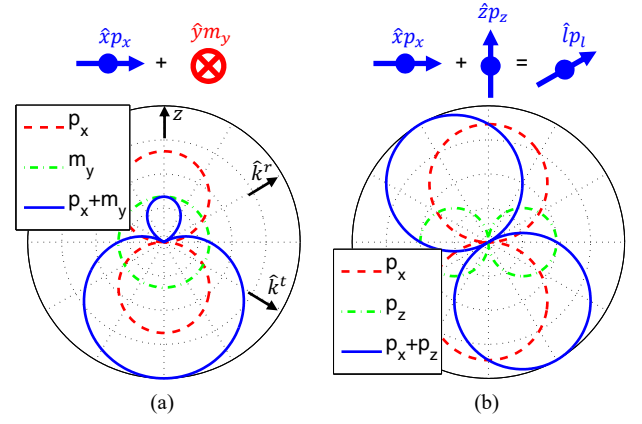


FIG. 3. Meta-atom scattering magnitude patterns for zero reflection at  $\theta^i = 60^\circ$ . (a) A combination of  $\hat{x}p_x$  and  $\hat{y}m_y$ . (b) A combination of  $\hat{x}p_x$  and  $\hat{z}p_z$ . The total pattern as well as the patterns of elemental dipoles are shown. The patterns are in linear scale with an arbitrary unit. All dipoles are treated as point dipoles.

At a design frequency  $\omega$ , the phase of  $r_s$  can be adjusted to any value in the range  $[-\pi, -\pi/2]$  or  $[\pi/2, \pi]$  by adjusting  $A_e$ ,  $\omega_e$ , and  $S$  of a resonant meta-atom. From (19), it can be seen  $\angle t$  has a full  $2\pi$  range.

It is instructive to inspect the physical conditions for zero reflection in terms of dipole moments. For a combination of  $\hat{x}p_x$  and  $\hat{y}m_y$ , setting  $r = r_s + r_a = 0$  using (5) and (11) gives

$$m_y + \eta p_x \cos \theta^i = 0. \quad (23)$$

In [40], extended relations of (23) between the electric and magnetic dipole amplitudes for a generalized Brewster effect in dielectric metasurfaces were derived for any given incidence angle, frequency, and polarization. For normal incidence ( $\theta^i = 0$ ), (23) corresponds to a zero backscattering condition (in the  $+z$ -axis direction). This condition for an orthogonal set of electric and magnetic dipoles has also been utilized in antenna designs [41, 42]. In the case of planar array or metasurface designs, zero specular reflection is of interest and (23) is the necessary condition at any incidence angle. In [43], the same balance condition was the principle behind thin Huygens sheet absorbers under a normal incidence. As an example, the element (meta-atom) scattering pattern of a balanced electric-magnetic dipole pair for a  $60^\circ$  incidence case is shown in Fig. 3(a). Together with the total pattern, the individual scattering patterns of  $\hat{x}p_x$  and  $\hat{y}m_y$  are also shown. In the specular reflection ( $\hat{k}^r$ ) direction, the two individual patterns destructively interfere to create a null, while they interfere constructively in the transmission ( $\hat{k}^t$ ) direction. The phases of the two moments  $p_x$  and  $m_y$  may be varied under the condition (23) to tune the transmission phase.

For a combination of  $\hat{x}p_x$  and  $\hat{z}p_z$ , the zero reflection condition translates to

$$p_x \cos \theta^i = p_z \sin \theta^i. \quad (24)$$

Hence, the two orthogonal induced dipole components should be in phase and their magnitudes should scale properly as a



function of  $\theta^i$ . The individual and total scattering patterns for a combination of two electric dipoles satisfying (24) are shown in Fig. 3(b) for the same  $60^\circ$  oblique illumination. A destructive interference creates a scattering null in the  $\hat{k}^r$  direction. As indicated in Fig. 3(b), this combination of two orthogonal dipoles corresponds to a single tilted electric dipole. Hence, there exists an interesting realization strategy in microwaves, where the direction of a low-loss conduction current can be accurately controlled by shaping thin conductors in meta-atoms. **Using a tilted straight dipole meta-atom to realize  $\hat{l}_p$  in Fig. 3(b), (24) will be satisfied for any value of  $p_l$ . The tangential and normal dipole moments will follow exactly the same frequency dispersion. The result is dispersionless zero reflection at the specific oblique incidence angle that matches the dipole tilt angle in the opposite direction. For lossless meta-atoms, this translates into dispersionless full transmission.** When volumetric electric polarization currents are utilized,  $\hat{x}p_x$  and  $\hat{z}p_z$  should be jointly designed to satisfy the proper magnitude and phase relations, i.e., (24). A microwave metasurface design based on the former strategy and an optical design based on the latter approach are presented in Sec. V.

It is stressed that using tangential and normal electric dipoles for creating reflectionless metasurfaces is limited to oblique illuminations in the TM polarization. At a normal incidence, the reflection direction is also normal to the surface. Even if the normal electric dipole,  $\hat{z}p_z$ , is induced by the incident wave, it cannot scatter in the reflection and transmission directions, which are the axial directions of  $\hat{z}p_z$ . In comparison, the combination of tangential electric and magnetic dipoles is available for any angle of incidence.

Since either a tangential magnetic dipole or a normal electric dipole can contribute to creating zero reflection together with a given tangential electric dipole, we can find a relation between  $m_y$  and  $p_z$  for contributing the same effect. By equating the values of  $r_a$  due to the two dipoles from (8) and (11), we find  $m_y = -\eta p_z \sin \theta^i$ , which can be written in the form

$$\hat{y}M_y = -\hat{n} \times \frac{\mathbf{k}_t}{\omega\epsilon_0} J_z; \quad \hat{n} = \hat{z}, \quad \mathbf{k}_t = \hat{x}k \sin \theta^i \quad (25)$$

in terms of surface-averaged polarizations. Here,  $\epsilon_0$  is the free-space permittivity and  $\hat{n}$ ,  $\mathbf{k}_t$  represent the unit surface normal and the tangential wave vector, respectively. Identified in [34], (25) represents an equivalence between a tangential magnetic polarization and a spatially-varying normal electric polarization.

#### IV. TRANSMISSION MAGNITUDE AND PHASE FOR LOSSY, REFLECTIONLESS METASURFACES

Absorption in lossy constituent materials is inevitable in practical realizations, resulting in reduction of the transmission power efficiency from 100%. On the other hand, zero reflection and zero transmission are desired for absorber applications. In this Section, we investigate if there is a limitation in designing the transmission phase when absorption is present and how the phase may be controlled.

Let the absorptance in the scattering described in Fig. 1 be denoted by  $A$  in the range  $0 < A < 1$ . It is defined as the absorbed power within a unit cell normalized by the incident power on the unit-cell area. Then, the power relation dictates  $|r|^2 + |t|^2 = 1 - A$ . Using the decompositions of  $r$  and  $t$  into the symmetric and anti-symmetric scattering components (13)–(14), this power conservation relation can be written in terms of  $t_s$  and  $r_a$  as

$$\text{Re}\{t_s + r_a\} - (|t_s|^2 + |r_a|^2) = \frac{A}{2}. \quad (26)$$

For both high-transmission and absorber applications, zero reflection is desirable. Using  $r_a = 1 - t_s$  in (26) gives

$$|t_s|^2 - \text{Re}\{t_s\} + \frac{A}{4} = 0. \quad (27)$$

The solution for  $|t_s|$  is readily found to be

$$|t_s| = \frac{\cos \phi_{t_s} \pm \sqrt{\cos^2 \phi_{t_s} - A}}{2}. \quad (28)$$

We find that the passivity and power conservation principles do not require a particular one of the two branches to be taken for the square root function in (28). Both values of  $|t_s|$  are valid solutions. For real-valued solutions to exist for  $|t_s|$ , it is required that  $\cos^2 \phi_{t_s} - A \geq 0$ . Hence, we find that  $t_s$  has its phase limited to the range

$$-\cos^{-1} \sqrt{A} \leq \phi_{t_s} \leq \cos^{-1} \sqrt{A}. \quad (29)$$

Using (28), the transmission coefficient is expressed as

$$t = e^{j\phi_{t_s}} \left( \pm \sqrt{\cos^2 \phi_{t_s} - A} + j \sin \phi_{t_s} \right). \quad (30)$$

If we carry out a similar analysis in terms of  $r_s$  instead of  $t_s$ , it is found that the range of  $\phi_{r_s}$  is limited to

$$\cos^{-1} \left( -\sqrt{A} \right) \leq |\phi_{r_s}| \leq \pi. \quad (31)$$

The transmission coefficient has an alternative expression given by

$$t = e^{j\phi_{r_s}} \left( \pm \sqrt{\cos^2 \phi_{r_s} - A} - j \sin \phi_{r_s} \right). \quad (32)$$

By allowing both branches in (30) and (32), it is easy to verify that the range of transmission phase is  $2\pi$  regardless of the value of  $A$ . Hence, we conclude that the presence of absorption does not fundamentally require the transmission phase range to be reduced from  $2\pi$  associated with the lossless case.

Using a lossy meta-atom model, we inspect the range of a realizable transmission phase and develop a design approach for achieving a particular combination of  $|t|$  and  $\angle t$ . A lossy meta-atom having a Lorentz-type resonant response can be modeled using a polarizability function given by

$$\alpha_{ee} = \frac{A_e}{\omega_e^2 - \omega^2 + j\gamma_e\omega}, \quad (33)$$

where  $\gamma_e$  is the electric loss factor or collision frequency. Using (5), (21), and (33), the transmission coefficient, written as  $t = 1 + 2r_s$  under a zero reflection condition, is expressed as

$$t = \frac{\frac{\omega_e^2 - \omega^2}{\eta A_e} + j\omega \left( \frac{\gamma_e}{\eta A_e} - \frac{\cos \theta^i}{2S} \right)}{\frac{\omega_e^2 - \omega^2}{\eta A_e} + j\omega \left( \frac{\gamma_e}{\eta A_e} + \frac{\cos \theta^i}{2S} \right)}. \quad (34)$$

For notational simplicity, let us introduce symbols  $u = \gamma_e \omega / \eta A_e$ ,  $v = \omega \cos \theta^i / 2S$ , and  $w = (\omega_e^2 - \omega^2) / \eta A_e$ . It is noted that  $u$  and  $v$  are positive quantities, but  $w$  can take any real value. Enforcing an absorptance value of  $A = 1 - |t|^2$  relates  $u$ ,  $v$ ,  $w$ , and  $A$ . The resulting value of  $w$  can be written in terms of the remaining quantities as

$$w = \pm \sqrt{2 \left( \frac{2}{A} - 1 \right) uv - u^2 - v^2}. \quad (35)$$

For  $w$  to be real-valued, the quantity under the square root should be non-negative. This defines the region of a valid point  $(u, v)$  in the  $uv$ -plane. It is found that the ratio  $u/v$  is bound between two constants defined by  $A$ , i.e.,

$$2 \left[ \frac{1}{A} - \sqrt{\frac{1}{A} \left( \frac{1}{A} - 1 \right)} \right] - 1 < \frac{u}{v} < 2 \left[ \frac{1}{A} + \sqrt{\frac{1}{A} \left( \frac{1}{A} - 1 \right)} \right] - 1. \quad (36)$$

Let us denote the lower and upper limits in (36) by  $s_0$  and  $s_1$ , respectively. It is noted that

$$0 < s_0 < 1, \quad s_1 > 1, \quad \text{and} \quad s_0 s_1 = 1, \quad (37)$$

for all possible values of  $A$ . In addition, let us introduce a slope function  $s$  as a function of a parameter  $q$  via

$$s(q) = s_0 + (s_1 - s_0)q, \quad 0 < q < 1, \quad (38)$$

so that  $u = s(q)v$ .

For the time being, let us assume that  $w > 0$  in (35). From (34), the transmission phase is expressed as

$$\angle t = \tan^{-1} \frac{u/v - 1}{|w|/v} - \tan^{-1} \frac{u/v + 1}{|w|/v}. \quad (39)$$

In (39), the quantity  $|w|/v$  is positive and  $|w|/v \rightarrow 0^+$  as  $s \rightarrow s_0, s_1$ . Now, we inspect the numerators in the argument of the arctangent functions in (39). For the second arctangent, it is seen that  $u/v + 1$  remains positive in  $0 < q < 1$  (i.e., its entire range) for all possible values of  $A$ . The numerator in the first arctangent function has a range

$$s_0 - 1 < \frac{u}{v} - 1 < s_1 - 1. \quad (40)$$

From (37), we note that the lower limit in (40) is a negative quantity, while the upper limit is a positive one, for all possible  $A$ . Hence, the first term in (39) changes from  $-\pi/2$  to  $\pi/2$  as

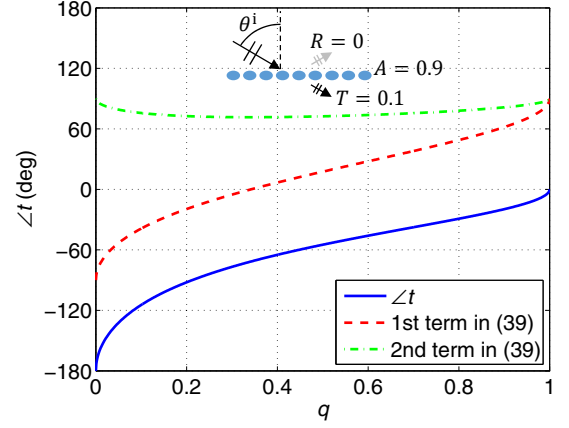


FIG. 4. Transmission phase design for a lossy, reflectionless metasurface with an absorptance of  $A = 0.9$ . The values of a reflectance  $R = 0$  and a transmittance  $T = 0.1$  are also indicated in the inset. The range of  $u/v$  for this example is equal to  $0.520 < u/v < 1.925$ .

$q$  is increased from 0 to 1. The second term in (39) stays in the range between 0 and  $\pi/2$ , but it reaches  $\pi/2$  at  $q = 0, 1$ . Hence, we expect a range of  $\pi$  for the transmission phase, in  $-\pi < \angle t < 0$ . For an example case of  $A = 0.9$ , Fig. 4 shows the transmission phase with respect to  $q$ . It can be seen that there exists a unique value of  $q$  for achieving a desired value of  $\angle t$ .

For synthesizing a transmission phase in  $-\pi < \angle t < 0$ , a meta-atom design strategy can be described as follows. For a given absorptance  $A$ , the transmission magnitude is fixed at  $|t| = \sqrt{1 - A}$  for a reflectionless response. The phase angle  $\angle t$  spans  $[-\pi, 0]$  as a function of  $u/v$  in  $s_0 < s < s_1$  ( $0 < q < 1$ ). Equation (39) can be solved for the value of  $q$  that achieves a desired transmission phase and the corresponding value of  $u/v$  follows. The associated value of  $w/v$  is obtained from (35). At the design frequency  $\omega$  and the incidence angle  $\theta^i$ , a meta-atom is designed by determining a combination of values for  $A_e$ ,  $\omega_e$ ,  $S$ , and  $\gamma_e$  for giving the determined ratios  $u/v$  and  $w/v$ .

A transmission phase in the range  $0 < \angle t < \pi$  can be designed using the negative branch for  $w$  in (35). For  $w < 0$ , we note from (34) that

$$\angle t = - \left( \tan^{-1} \frac{u/v - 1}{|w|/v} - \tan^{-1} \frac{u/v + 1}{|w|/v} \right), \quad (41)$$

which is an opposite number for (39). Therefore, to design a value of  $\angle t$  in  $[0, \pi]$ , meta-atom parameters can be first determined for achieving a phase of  $-\angle t$ , following the approach described above for realizing a transmission phase in  $[-\pi, 0]$ . Then, the sign of  $w$  needs to be changed, which can be achieved by setting  $\omega_e < \omega$ , i.e., by choosing the resonance frequency of the lossy meta-atom lower than the design frequency.

Combining the two separate cases of the desired transmission phase being in  $[-\pi, 0]$  or  $[0, \pi]$ , we conclude that a reflectionless metasurface can be designed using lossy meta-atoms following the Lorentz dispersion model to achieve a transmis-

sion phase in a full  $2\pi$  range at any level of absorption at any oblique angle of incidence.

## V. NUMERICAL EXAMPLES

In this section, we will present different alternatives for Huygens' metasurfaces where the tangential and normal electric dipole moments are carefully engineered for satisfying the reflectionless condition while providing a complete transmission phase coverage. We will explore the possibilities for the design of metasurfaces at microwave and optical frequencies for lossless and lossy scenarios.

### A. Reactively-loaded tilted thin conductor strip dipole array

At microwave frequencies, the direction of induced electric dipole moments can be easily controlled using thin conductor wires and traces. For supporting both tangential and normal electric dipoles, a straight thin conductor dipole can be tilted to produce zero reflection. Here, it is noted that (24) is the zero reflection condition for point dipoles. For meta-atoms of practical dimensions, zero reflection corresponds to a scattering pattern null in the specular reflection direction. For a straight conductor dipole of any length, aligning the dipole axis in the specular reflection direction guarantees  $r = 0$ . The transmission characteristics of a tilted straight dipole array are analyzed in Fig. 5. For a TM-polarized plane-wave illumination at an incidence angle of  $60^\circ$ , a perfect electric conductor (PEC) strip dipole tilted at the same  $60^\circ$  angle in the opposite direction constitutes the meta-atom, as shown in the inset of Fig. 5(a). At the middle point of the dipole, a lumped load with an impedance  $Z_l$  is connected. While providing tunability for  $t$ , such a load does not affect the reflectionless property. At a design frequency of 5 GHz, the unit-cell dimensions are chosen to be  $a = b = 20$  mm, so that there are no higher-order propagating Floquet modes. For an electrically thin width of  $w = 0.6$  mm, the length of the strip was adjusted to  $l = 29.9$  mm such that the transmission phase for the unloaded case ( $Z_l = 0$ ) is equal to  $\pi$ . The dipole meta-atom extends slightly into neighboring cells. Using a phase-shift periodic boundary condition (PBC) on the four vertical walls of the unit cell, the scattering characteristics of an infinitely large planar array were simulated using FEKO 2017 by Altair.

At the design frequency, the magnitude and phase of  $t$  are plotted in Fig. 5(a) with respect to the reactance  $X_l$  of the reactive load impedance  $Z_l = jX_l$ . Since the meta-atom is lossless and the dipole does not reflect, the transmission magnitude is constant at unity. By loading the dipole with different reactance  $X_l$ , the transmission phase can be adjusted to any value in the range  $-\pi < \angle t \leq \pi$ . Not the entire  $2\pi$  phase range is visible in Fig. 5(a). Simulations with large loading reactances show that the transmission phase approaches a single value of  $\angle t = -19.6^\circ$  from different directions as  $X_l \rightarrow \pm\infty$ . Considering that the dipole meta-atom is not electrically short, large loading reactances will not make it ef-

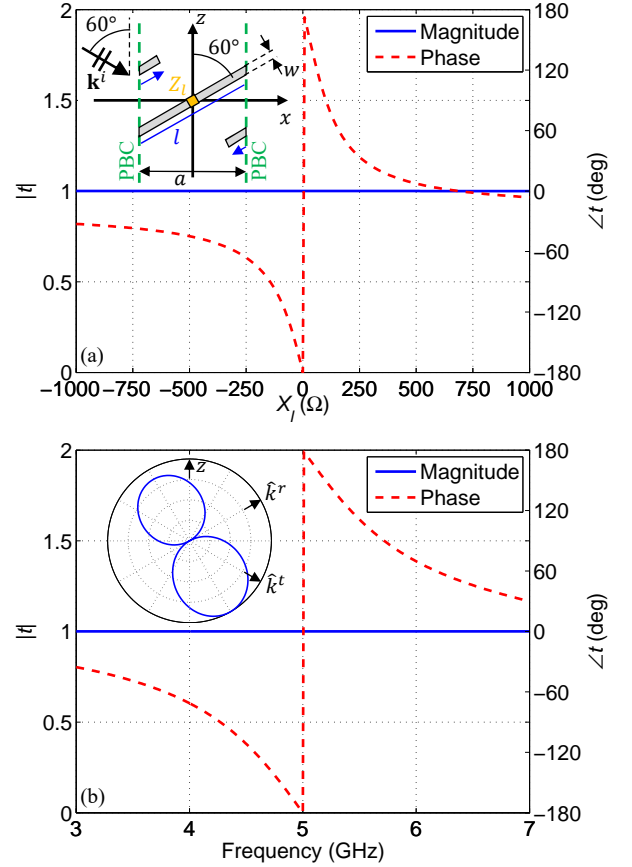


FIG. 5. Plane wave scattering by a planar array of tilted conductor strip dipoles. The meta-atom comprises a conducting strip dipole of dimensions  $l \times w$ . The plane of the strip is the  $xz$ -plane and the strip surface is assumed to be perfectly conducting. A point load with a reactive impedance  $Z_l = jX_l$  is connected at the dipole middle point. (a) The transmission magnitude and phase with respect to the load reactance  $X_l$  at 5 GHz. The inset shows a side view of the unit cell together with the illuminating plane wave. (b) The transmission coefficient as a function of frequency when the load port is shorted ( $X_l = 0$ ). The unit-cell dimension is  $a = 20$  mm in both  $x$ - and  $y$ -axis directions. The length and width of the strip dipole are  $l = 29.9$  mm and  $w = 0.6$  mm. The unit-cell scattering pattern at 5 GHz is shown in the inset.

fectively non-existent. Instead, the meta atom will appear as two narrowly separated collinear dipoles of a length  $l/2$  each.

For an unloaded dipole ( $X_l = 0$ ), Fig. 5(b) plots the transmission coefficient with respect to frequency. A standard Lorentz-type resonant frequency response is observed for the phase. In the inset, the normalized unit-cell scattering pattern at 5 GHz in the  $xz$ -plane is shown as a polar plot. The length of the dipole meta-atom of nearly a half wavelength makes the pattern deviate noticeably from that of a point dipole shown in Fig. 3(b). Still, a scattering null is synthesized in the reflection direction due to the tilt. In this design, the bandwidth of full power transmission is in principle infinite. This is due to satisfaction of the no reflection condition of a geometrical origin. For a tilted straight dipole, the normal and tangential surface-averaged electric polarizations,  $J_x = j\omega p_x/S$ ,  $J_z = j\omega p_z/S$ ,

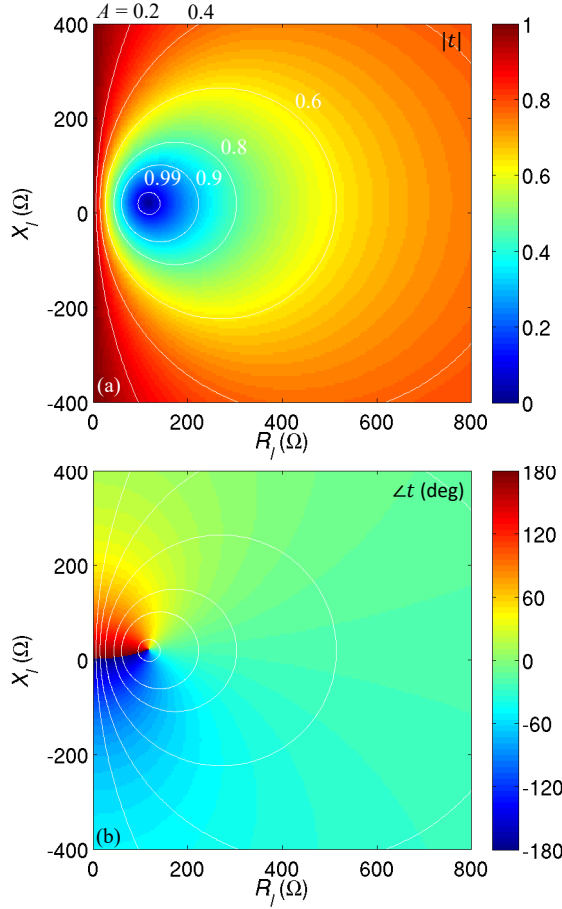


FIG. 6. The transmission coefficient with respect to the lumped load resistance  $R_l$  and reactance  $X_l$  values. (a) The magnitude. (b) The phase angle in degrees. The white contour lines correspond to different absorbance values of  $A = \{0.2, 0.4, 0.6, 0.8, 0.9, 0.99\}$ . The  $A = 0$  contour is the  $R_l = 0$  axis.

have the exact same frequency dispersion. If zero reflection is achieved via a balance of electric and equivalent magnetic polarizations as is done in Huygens' metasurfaces, the high-transmission frequency bandwidth is not expected to be wide.

### B. Impedance-loaded tilted strip dipole array

To the tilted conductor dipole array of Sec. V A, loss can be introduced to make the metasurface absorptive. For this purpose, a resistive component can be incorporated into the load impedance  $Z_l$  in Fig. 5(a). At the same time, adjusting the reactance part is expected to give a capability to tune the transmission phase. To the tilted PEC strip dipole array considered in Sec. V A, a complex load with an impedance  $Z_l = R_l + jX_l$  is attached to the center point of the meta-atom. In the range  $0 \leq R_l \leq 800 \Omega$ ,  $-400 \Omega \leq X_l \leq 400 \Omega$ , the reflection and transmission coefficients were simulated using FEKO at 5 GHz. The simulated reflection coefficient is zero. The transmission coefficient is shown in Fig. 6. The magnitude plot in Fig. 6(a) demonstrates that the entire range

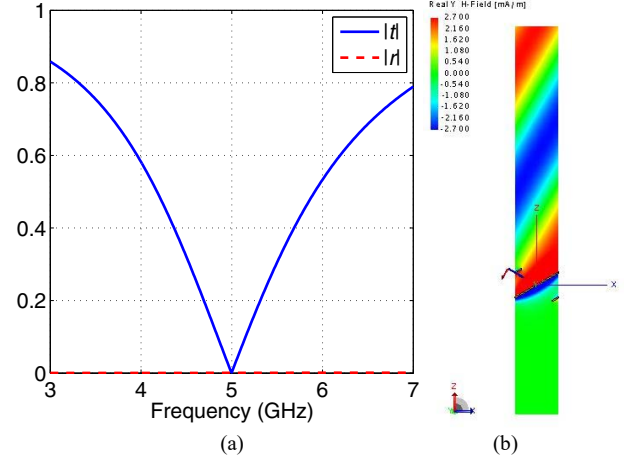


FIG. 7. Characteristics of the center-loaded strip dipole array with the load impedance chosen for perfect absorption at 5 GHz. (a) The magnitude of the reflection and transmission coefficients with respect to frequency. (b) A snapshot of the total  $y$ -directed magnetic field,  $H_y$ .

of  $|t|$  between zero and unity is available for synthesis. For visualization, a few contours for constant- $|t|$  (in terms of the absorbance  $A$ ) values are also plotted. The same contours are reproduced in Fig. 6(b), where the transmission phase is plotted. It is clear that for any given value of  $A$ , an arbitrary phase in a complete  $2\pi$  range can be achieved in principle by selecting an appropriate value for  $Z_l$ . In practice, extreme values of  $R_l$ ,  $X_l$  required for some combinations of  $|t|$  and  $\angle t$  may be difficult to realize and consequently limit the synthesis range.

In Fig. 6(a), an extreme case of full absorption is observed with a selection of load impedance  $Z_l = 115.9 + j20.6 \Omega$ . If the received power is guided to a receiving circuitry rather than dissipated as heat, the design corresponds to a planar receiving array with a 100% receiving efficiency. The frequency responses of  $|r|$  and  $|t|$  are shown in Fig. 7(a). The metasurface does not transmit nor reflect at the design frequency of 5 GHz. The bandwidth is reflection zero is extremely wide. At 5 GHz, a snapshot at time  $t = 0$  of the  $y$ -component of the total magnetic field in the  $xz$ -plane is plotted over the unit-cell dimension of  $-a/2 < x < a/2$  in Fig. 7(b). Only the fields associated with the incident wave is visible above the metasurface and zero field penetrates behind the dipole array.

In this design, absorption occurs at the load connected to the otherwise lossless meta-atom. Instead, it is possible to design an absorber based on a distributed loss mechanism. One approach will be realizing the dipole meta-atom using lossy conductive material such as conductive ink films, modeled as a resistive impedance sheet [44]. Such a lossy strip array variant was designed for perfect absorption at 5 GHz and numerically analyzed. Its simulated scattering characteristics exhibit the same qualitative behavior presented in Fig. 7 (not shown).



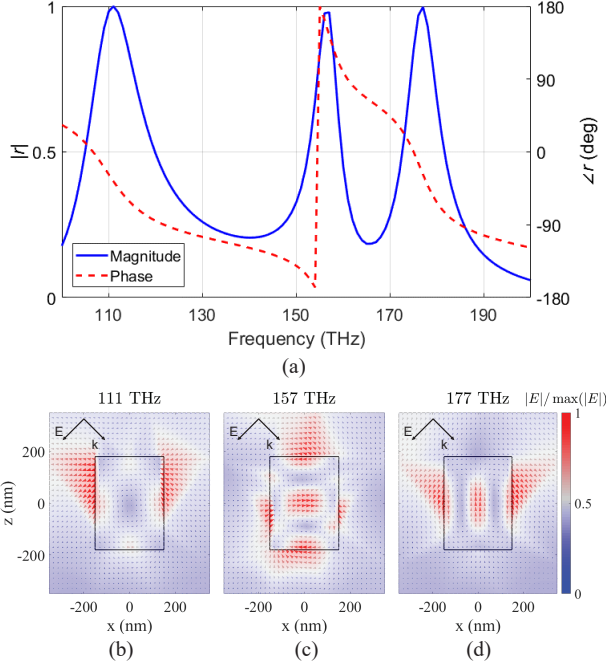


FIG. 8. Scattering by an array of dielectric bars illuminated obliquely at an incidence angle of  $\theta^i = 45^\circ$ . The refractive index of the dielectric material is  $n_d = 6$ , the periodicity is  $a = 730$  nm, the width is  $w = 300$  nm and the height is  $h = 360$  nm. (a) Reflection spectrum. (b-d) Field distributions at the three resonant frequencies: (b) A tangential magnetic dipole; (c) A tangential electric dipole; (d) A vertical electric dipole.

### C. Array of dielectric bars of rectangular cross section

Here we give an example of a high-transmission array offering full control of the transmission phase in the optical domain. In order to ensure small dissipation losses, we use an all-dielectric metasurface formed by an array of parallel bars made of a lossless high refractive index dielectric ( $n_d = 6$ ) with the axis of the bars oriented along the  $y$ -direction. Due to the 2-D nature of the problem, the  $y$ -periodicity is infinite so we ensure the absence of higher order modes propagating in this direction. In conventional realizations of high-transmission all-dielectric metasurfaces, the Huygens regime is realized by exciting both electric and magnetic moments at the operational frequency. Here, we illuminate the array by an obliquely propagating plane wave to ensure excitation of both tangential and normal electric polarizations and utilize the theory in this paper to realize a full transmission with a complete phase control. Following the previous example, we consider a TM-polarized incident plane wave [see Fig. 9(a)] and we define the incidence angle to be  $45^\circ$ .

The reflection spectrum is presented in Fig. 8(a) when the periodicity is  $a = 730$  nm, the width is  $w = 300$  nm and the height is  $h = 360$  nm. It exhibits three reflection maxima which correspond to three dipole-mode resonances. The first reflection peak, at 111 THz, corresponds to a tangentially oriented magnetic dipole. Figure 8(b) shows the electric field

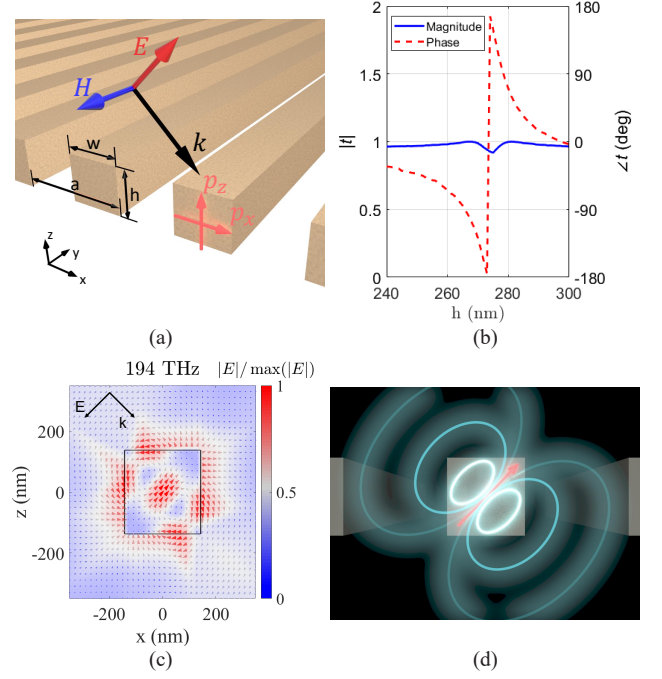


FIG. 9. A high-transmission all-dielectric array utilizing induced electric dipoles. (a) Schematic of the studied structure: an array of dielectric bars with a refractive index  $n_d = 6$  illuminated at an angle of  $\theta^i = 45^\circ$ . (b) Transmission amplitude and phase of arrays of bars at a frequency of 194 THz with different shape parameters. The periodicity of the bars is kept constant,  $a = 730$  nm, and the width of the bars is  $w = h + 10$  nm. (c) An electric field distribution at 194 THz for  $h = 275$  nm. (d) A conceptual illustration of the induced dipole moment.

vector in the  $xz$ -plane, where we can see that the electric field circulates inside the bars generating an out-of-plane magnetic dipole moment. At 157 THz, the reflection peak is caused by the resonance of a tangential electric dipole, as we can see in Fig. 8(c). The third resonance peak, at 177 THz, corresponds to the resonance of a normal electric dipole [see Fig. 8(d)]. Adjusting the shape parameters of the bars, the magnitude and phase of the induced dipoles can be tuned to fulfill the conditions in (24).

Finally, a combination of  $\hat{x}p_x$  and  $\hat{z}p_z$  can be tuned to transmit the incident light with required phase variations within the  $2\pi$  range. We consider a periodic array as shown in Fig. 9(a) with a period  $a = 730$  nm. The bars have a rectangular cross section with a height  $h$  and a width  $w = h + 10$  nm. Figure 9(b) shows the transmission magnitude and phase for arrays of bars of different sizes, as a function of  $h$ . We see that the transmission phase indeed varies within the full  $2\pi$  range while the transmission magnitude remains close to unity. Figures 9(c,d) show the calculated field distribution and a conceptual illustration of an excited tilted electric dipole moment for  $h = 275$  nm. The simulations were performed using ANSYS HFSS, setting PBCs on the vertical walls of the unit cell.

For absorptive applications, an array of dielectric bars made from a suitable lossy material is a straightforward extension of the high-transmission array in Fig. 9. An optical analogue of

the array of tilted dipoles in Sec. VB is another possibility. Using the approach of lossy surface impedance realization in [45] exploiting the surface dispersion of nanoparticles, it can be envisaged that metal nanoparticles are deposited on some dielectric support having periodic slanted walls. The tilt angle of the dielectric support can enforce (24). The surface resistance may be designed to achieve various levels of absorption, including complete absorption. This approach needs further investigation.

## VI. CONCLUSION

For polarization-preserving transmissive metasurface, it has been shown that the origin of a full transmission capability together with a complete  $2\pi$  phase coverage is synthesis of an asymmetric scattering pattern with respect to the metasurface plane. In Huygens' meta atoms, a tangential magnetic dipole is responsible for creating anti-symmetric scattering. An alternative meta-atom arrangement is available for full transmis-

sion in oblique TM-polarization scattering, as a combination of tangential and normal electric dipoles. A particular realization is an array of tilted straight conductor dipole meta-atoms with the dipole axis aligned with the reflection direction. The geometrical nature of the synthesized scattering null allows an extremely wide bandwidth of zero reflection. In the presence of loss in constituent materials or intended power absorption, it has been analytically proven and demonstrated using a numerical example that a complete transmission phase coverage is possible for reflectionless metasurfaces. The operation principle and the new design strategy presented in this study will facilitate development of a new class of transmissive metasurfaces for wave manipulation with high power efficiencies.

## ACKNOWLEDGMENT

This work was supported in part by the Academy of Finland (project 287894).

- 
- [1] C. L. Holloway, E. F. Kuester, J. A. Gordon, J. O'Hara, J. Booth, and D. R. Smith, "An overview of the theory and applications of metasurfaces: the two-dimensional equivalents of metamaterials," *IEEE Antennas Propag. Mag.* **54**, 10 (2012).
  - [2] A. V. Kildishev, A. Boltasseva, and V. M. Shalaev, "Planar photonics with metasurfaces," *Science* **339**, 1232009 (2013).
  - [3] N. Yu and F. Capasso, "Flat optics with designer metasurfaces," *Nat. Mater.* **13**, 139 (2014).
  - [4] N. Meinzer, W. L. Barnes, and I. R. Hooper, "Plasmonic meta-atoms and metasurfaces," *Nat. Photon.* **8**, 889 (2014).
  - [5] S. B. Glybovski, S. A. Tretyakov, P. A. Belov, Y. S. Kivshar, and C. R. Simovski, "Metasurfaces: From microwaves to visible," *Phys. Rep.* **634**, 1 (2016).
  - [6] H.-T. Chen, A. J. Taylor, and N. Yu, "A review of metasurfaces: physics and applications," *Rep. Prog. Phys.* **79**, 076401 (2016).
  - [7] R. C. Hansen, *Phased Array Antennas*, 2nd ed. (Wiley, Hoboken, NJ, 2009).
  - [8] N. Yu, P. Genevet, M. A. Kats, F. Aieta, J.-P. Tetienne, F. Capasso, and Z. Gaburro, "Light propagation with phase discontinuities: generalized laws of reflection and refraction," *Science* **334**, 333 (2011).
  - [9] C. Pfeiffer and A. Grbic, "Metamaterial Huygens' surfaces: tailoring wave fronts with reflectionless sheets," *Phys. Rev. Lett.* **110**, 197401 (2013).
  - [10] F. Aieta, P. Genevet, N. Yu, M. A. Kats, Z. Gaburro, and F. Capasso, "Out-of-plane reflection and refraction of light by anisotropic optical antenna metasurfaces with phase discontinuities," *Nano Lett.* **12**, 1702 (2012).
  - [11] C. Pfeiffer, N. K. Emani, A. M. Shaltout, A. Boltasseva, V. M. Shalaev, and A. Grbic, "Efficient light bending with isotropic metamaterial Huygens' surfaces," *Nano Lett.* **14**, 2491 (2014).
  - [12] Y. F. Yu, A. Y. Zhu, R. Paniagua-Domínguez, Y. H. Fu, B. Luk'yanchuk, and A. I. Kuznetsov, "High-transmission dielectric metasurface with  $2\pi$  phase control at visible wavelengths," *Laser Photon. Rev.* **9**, 412 (2015).
  - [13] F. Monticone, N. Mohammadi Estakhri, and A. Alù, "Full control of nanoscale optical transmission with a composite metascreen," *Phys. Rev. Lett.* **110**, 203903 (2013).
  - [14] D. Lin, P. Fan, E. Hasman, and M. L. Brongersma, "Dielectric gradient metasurface optical elements," *Science* **345**, 298 (2014).
  - [15] Q. Wang, X. Zhang, Y. Xu, Z. Tian, J. Gu, W. Yue, S. Zhang, J. Han, and W. Zhang, "A broadband metasurface-based terahertz flat-lens array," *Adv. Opt. Mater.* **3**, 779 (2015).
  - [16] M. Khorasaninejad, W. T. Chen, R. C. Devlin, J. Oh, A. Y. Zhu, and F. Capasso, "Metalenses at visible wavelengths: Diffraction-limited focusing and subwavelength resolution imaging," *Science* **362**, 1190 (2016).
  - [17] X. Ni, A. V. Kildishev, and V. M. Shalaev, "Metasurface holograms for visible light," *Nat. Commun.* **4**, 2087 (2013).
  - [18] L. Huang, X. Chen, H. Mühlenbernd, H. Zhang, S. Chen, B. Bai, Q. Tan, G. Jin, K.-W. Cheah, C.-W. Qiu, J. Li, T. Zentgraf, and S. Zhang, "Three-dimensional optical holography using a plasmonic metasurface," *Nat. Commun.* **4**, 2808 (2013).
  - [19] A. Arbabi, Y. Horie, M. Bagheri, and A. Faraon, "Dielectric metasurfaces for complete control of phase and polarization with subwavelength spatial resolution and high transmission," *Nat. Nanotechnol.* **10**, 937 (2015).
  - [20] Y. Zhao, M. A. Belkin, and A. Alù, "Twisted optical metamaterials for planarized ultrathin broadband circular polarizers," *Nat. Commun.* **3**, 870 (2012).
  - [21] C. Pfeiffer and A. Grbic, "Millimeter-wave transmitarrays for wavefront and polarization control," *IEEE Trans. Microw. Theory Techn.* **61**, 4407 (2013).
  - [22] N. K. Grady, J. E. Heyes, D. R. Chowdhury, Y. Zheng, M. T. Reiten, A. K. Azad, A. J. Taylor, D. A. R. Dalvit, and H.-T. Chen, "Terahertz metamaterials for linear polarization conversion and anomalous refraction," *Science* **340**, 1304 (2013).
  - [23] F. Aieta, P. Genevet, M. A. Kats, N. Yu, R. Blanchard, Z. Gaburro, and F. Capasso, "Aberration-free ultrathin flat lenses and axicons at telecom wavelengths based on plasmonic metasurfaces," *Nano Lett.* **12**, 4932 (2012).
  - [24] G. Zheng, H. Mühlenbernd, M. Kenney, G. Li, T. Zentgraf, and S. Zhang, "Metasurface holograms reaching 80% efficiency," *Nat. Nanotech.* **10**, 308 (2015).

- [25] M. I. Shalaev, J. Sun, A. Tsukernik, A. Pandey, K. Nikolskiy, and N. M. Litchinitser, "High-efficiency all-dielectric metasurfaces for ultracompact beam manipulation in transmission mode," *Nano Lett.* **15**, 6261 (2015).
- [26] M. Decker, I. Staude, M. Falkner, J. Dominguez, D. N. Neshev, I. Brener, T. Pertsch, and Y. S. Kivshar, "High-efficiency dielectric Huygens' surfaces," *Adv. Optical Mater.* **3**, 813 (2015).
- [27] K. E. Chong, L. Wang, I. Staude, A. R. James, J. Dominguez, S. Liu, G. S. Subramania, M. Decker, D. N. Neshev, I. Brener, and Y. S. Kivshar, "Efficient polarization-insensitive complex wavefront control using Huygens' metasurfaces based on dielectric resonant meta-atoms," *ACS Photon.* **3**, 514 (2016).
- [28] J. P. S. Wong, M. Selvanayagam, and G. V. Eleftheriades, "Polarization considerations for scalar Huygens metasurfaces and characterization for 2-D refraction," *IEEE Trans. Microw. Theory Techn.* **63**, 913 (2015).
- [29] A. Epstein and G. V. Eleftheriades, "Huygens' metasurfaces via the equivalence principle: design and applications," *J. Opt. Soc. Am. B* **33**, A31 (2016).
- [30] T. Cai, S. Tang, G. Wang, H. Xu, S. Sun, Q. He, and L. Zhou, "High-performance bifunctional metasurfaces in transmission and reflection geometries," *Adv. Opt. Mater.* **5**, 1600506 (2017).
- [31] W. Luo, S. Sun, H.-X. Xu, Q. He, and L. Zhou, "Transmissive ultrathin Pancharatnam-Berry metasurfaces with nearly 100% efficiency," *Phys. Rev. Appl.* **7**, 044033 (2017).
- [32] T. Cai, G. Wang, S. Tang, H. Xu, J. Duan, H. Guo, F. Guan, S. S. Q. He, and L. Zhou, "High-efficiency and full-space manipulation of electromagnetic wave fronts with metasurfaces," *Phys. Rev. Appl.* **8**, 034033 (2017).
- [33] T. Niemi, A. O. Karilainen, and S. A. Tretyakov, "Synthesis of polarization transformers," *IEEE Trans. Antennas Propag.* **61**, 3102 (2013).
- [34] M. Albooyeh, D.-H. Kwon, F. Capolino, and S. A. Tretyakov, "Equivalent realizations of reciprocal metasurfaces: role of tangential and normal polarization," *Phys. Rev. B* **95**, 115435 (2017).
- [35] X.-R. Huang, R.-W. Peng, and R.-H. Fan, "Making metals transparent for white light by spoof surface plasmons," *Phys. Rev. Lett.* **105**, 243901 (2010).
- [36] A. Alù, G. D'Aguanno, N. Mattiucci, and M. J. Bloemer, "Plasmonic Brewster angle: broadband extraordinary transmission through optical gratings," *Phys. Rev. Lett.* **106**, 123902 (2011).
- [37] R.-H. Fan, R.-W. Peng, X.-R. Huang, J. Li, Y. Liu, Q. Hu, M. Wang, and X. Zhang, "Transparent metals for ultrabroadband electromagnetic waves," *Adv. Mater.* **24**, 1980 (2012).
- [38] C. F. Bohren and D. R. Huffman, *Absorption and Scattering of Light by Small Particles* (Wiley-VCH, Weinheim, Germany, 2004).
- [39] V. S. Asadchy, I. A. Faniayeu, Y. Ra'di, S. A. Khakhomov, I. V. Semchenko, and S. A. Tretyakov, "Broadband reflectionless metasheets: frequency-selective transmission and perfect absorption," *Phys. Rev. X* **5**, 031005 (2015).
- [40] R. Paniagua-Domínguez, Y. F. Yu, A. E. Miroshnichenko, L. A. Krivitsky, Y. H. Fu, V. Valuckas, L. Gonzaga, Y. T. Toh, A. Y. S. Kay, B. Luk'yanchuk, and A. I. Kuznetsov, "Generalized Brewster effect in dielectric metasurfaces," *Nat. Commun.* **7**, 10362 (2016).
- [41] R. B. Green, "Scattering from conjugate-matched antennas," *IEEE Trans. Antennas Propag.* **AP-14**, 17 (1966).
- [42] P. Jin and R. W. Ziolkowski, "Metamaterial-inspired, electrically small Huygens sources," *IEEE Antennas Wireless Propag. Lett.* **9**, 501 (2010).
- [43] Y. Ra'di, C. R. Simovski, and S. A. Tretyakov, "Thin perfect absorbers for electromagnetic waves: theory, design, and realizations," *Phys. Rev. Appl.* **3**, 037001 (2015).
- [44] X.-C. Wang, A. Díaz-Rubio, and S. A. Tretyakov, "An accurate method for measuring the sheet impedance of thin conductive films at microwave and millimeter-wave frequencies," *IEEE Trans. Microw. Theory Techn.* **65**, 5009 (2017).
- [45] A. Monti, A. Toscano, and F. Bilotti, "Exploiting the surface dispersion of nanoparticles to design optical-resistive sheets and Salisbury absorbers," *Opt. Lett.* **41**, 3383 (2016).